Effect of Blade Row Interaction on Rotor Film Cooling

J. Brind*, **G. Pullan**

Whittle Laboratory

Department of Engineering

University of Cambridge

Cambridge, CB3 0DY, UK

Email: jb753@cam.ac.uk

ABSTRACT

The mechanisms of blade row interaction affecting rotor film cooling are identified in order to make recommendations for the design of film cooling in the real, unsteady turbine environment. Present design practice makes the simplifying assumption of steady boundary conditions, despite intrinsic unsteadiness due to blade row interaction; we argue that if film cooling responds non-linearly to unsteadiness, the time-averaged performance will then be in error. Non-linear behaviour is confirmed using experimental measurements of flat-plate cylindrical film cooling holes, main-stream unsteadiness causing a reduction in film effectiveness of up to 31% at constant time-averaged boundary condition. Unsteady computations are used to identify the blade row interaction mechanisms in a high-pressure turbine rotor: a 'negative jet' associated with the upstream vane wake, and frozen and propagating vane potential field interactions. A quasi-steady model is used to predict unsteady excursions in momentum flux ratio of rotor cooling holes, with fluctuations of at least $\pm 30\%$ observed for all hole locations. Computations with modified upstream vanes are used to vary the relative strength of wake and potential field interactions. In general, both mechanisms contribute to rotor film cooling unsteadiness. It is recommended that the designer should choose a cooling configuration which behaves linearly over the expected unsteady excursions in momentum flux ratio as predicted by a quasi-steady hole model.

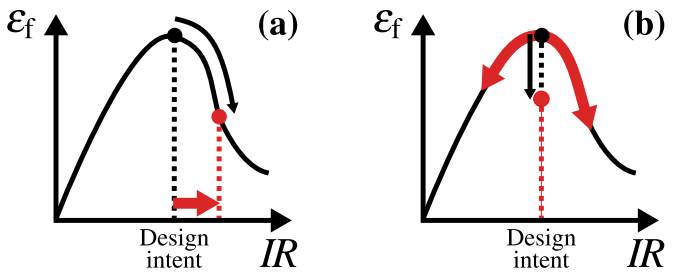

Fig. 1: Notional film effectiveness–momentum flux ratio characteristic for a film cooling hole. Time-averaged film effectiveness is altered by **(a)** a change in time-averaged boundary condition, and **(b)** movement on non-linear characteristic.

*Address all correspondance to this author.

INTRODUCTION

The possibility for unsteady blade row interaction to affect rotor film cooling performance has been recognised for some time, since the first measurements of film effectiveness on rotating blades showed discrepancies compared to predictions based on cascade and flat-plate measurements [1, 2]. According to the review by Bunker [3], the effect of unsteady flows remains an unquantified unknown in turbine cooling design.

In steady flow, a change in boundary condition, say, momentum flux ratio, *IR*, results in a change in film effectiveness, ε_f, according to the hole characteristic as shown in Fig. 1(a). In unsteady flow, the time-averaged film effectiveness is also affected by fluctuations about the time-averaged boundary condition, if the characteristic is non-linear as in Fig. 1(b). Present design methods assuming steady flow predict changes in time-averaged boundary condition, but are unable to capture non-linear effects.

The paper is organised into three parts. In the first part, measurements of flat-plate film cooling subject to main-stream unsteadiness are used to confirm non-linear behaviour as in Fig. 1(b). In the second part, turbine stage computations are used to identify mechanisms of blade row interaction and provide physical understanding of how rotor cooling is affected. In the third part, unsteady excursions in momentum flux ratio are quantified using a quasi-steady cooling hole model. Finally, the results are used to make recommendations for the design of rotor film cooling in the unsteady turbine environment.

BACKGROUND

In this section, relevant previous work is summarised and used to frame the contributions of the current paper. The effect of blade row interaction on film cooling has been investigated in non-rotating flat plate and cascade rigs, and rotating turbine stage rigs, which will be discussed in turn.

Artificial unsteadiness experiments

In non-rotating experiments, blade row interaction must be modelled using simulated, artificial unsteadiness. The unsteady boundary conditions on the cooling holes are then a particular idealisation of real blade row interaction.

The most common idealisation is the use of a moving-bar wake generator to simulate upstream vane wake interaction. Adding wakes has been shown to reduce film effectiveness, with both cylindrical holes [4, 5] and fan-shaped holes [6]. The reported quantitative effect on time-averaged cooling performance varies, but a reduction of up to 30% in laterally-averaged film effectiveness is typical. It has also been reported that the addition of wakes can improve the effectiveness of cylindrical holes, where coolant would be lifted-off in steady state, by up to 100% [6, 7]. Some studies find that the effect increases with wake passing frequency [7, 8]. Qualitatively, the wake effect is identical to an increased steady main-stream turbulence intensity [6].

A second idealised boundary condition is a static pressure oscillation, modelling interactions between vane potential field and rotor film cooling. Ligrani et al. [9] measured the effects of main-stream static pressure oscillations, generated by downstream rotating shutters, on film cooling effectiveness. With oscillations, the centreline film effectiveness reduced by up to 12% compared to steady flow. Seo et al. [10] studied the additional effect of hole length-to-diameter ratio, L/D, using the same apparatus. It was found that for short holes, $L/D = 1.75$, with separated coolant oscillations acted to increase the

centreline film effectiveness by up to 37% compared to steady flow. It is stated that the oscillations act to reduce coolant lift-off over part of the forcing cycle, whereas in steady state the jet is always lifted off. As these cases have the same time-averaged boundary conditions, this is a non-linear effect.

The general implications of these studies for the design process are unclear. Direct measurement of the amplitude of main-stream unsteadiness is not usually reported, and, often, measurable effects on film effectiveness occur only at amplitudes and reduced frequencies exceeding representative values. It is also difficult to isolate changes in time-averaged flow from from truly unsteady, non-linear effects in such experiments.

Turbine stage experiments

Abhari and Epstein [11] performed measurements of time-resolved heat flux in a transonic cooled turbine stage rotor, and measurements of a cooled cascade of the rotor blade profile. The heat flux to the rotor suction side is lower than the cascade, by up to 60%. It is noted that main-stream static pressure fluctuations are of the same order as the time-averaged coolant dynamic head, which causes fluctuations in coolant mass flow. A model for this behaviour was developed, where the instantaneous coolant mass flow is approximated and used as input to a film effectiveness correlation, which is then convected downstream. The local instantaneous film effectiveness is then used to correct measured values of uncooled heat fluxes. This model reproduces the qualitative features of the cooled heat fluxes: the measured data show that film cooling reduces the time-averaged value, and introduces a phase shift in the fluctuations.

Abhari [12] performed further experiments and simulations on the same turbine. A more complicated injection model, based on a series of correlations, was incorporated into a two dimensional, unsteady, coupled Euler/Navier-Stokes CFD solver. An unsteady calculation predicts time-averaged heat fluxes on the pressure side up to a factor of two higher than a steady mixing-plane calculation, due to a reduction of up to 64% in film effectiveness. Change in the mean coolant mass flow is found to account for 55% of this discrepancy, with the rest attributed to non-linear effects. Time-averaged heat fluxes on the suction side matched to within 5%, with the discrepancy due to non-linear effects alone.

The works by Abhari and Epstein [11] and Abhari [12] are, in the literature, the only unsteady film cooling investigations with complete turbine stage geometry and boundary conditions. However, their conclusions are mostly specific to the studied turbine, with less analysis of the general mechanisms at work.

Contributions of the present work

The view of the authors is that an understanding of the complete non-idealised turbine boundary conditions, and the general mechanisms by which they affect rotor film cooling, is necessary to apply previous work to practical designs. This paper addresses the research need for design recommendations by making three contributions:

1. Experimental confirmation that the effect of main-stream unsteadiness on film cooling is determined by non-linearity in the steady hole characteristic;
2. Qualitative characterisation of the blade row interaction mechanisms that affect rotor film cooling performance, based on an analysis of turbine stage computations;
3. Quantification of the effect of each interaction mechanism using a quasi-steady model for cooling hole behaviour.

The remainder of the paper is structured as follows. First, the conceptual approach used to quantify effects on rotor film cooling is described. Then, results covering the points above are presented in three parts.

CONCEPTUAL APPROACH

In this section, the approach used to assess the effect of blade row interaction on rotor film cooling is outlined. The overall modelling framework is illustrated in the diagram of Fig. 2, and the components are described in the proceeding sections. The quasi-steady assumption is discussed first, followed by the non-film-resolved computations which model the main-stream flow. Finally, the unsteady hole response model is presented.

Quasi-steady assumption

The parameter which characterises the importance of unsteady effects in a given flow is the reduced frequency, κ. For a rotor cooling hole, this can be defined as a ratio of the two characteristic time scales,

$$\kappa = \frac{\text{coolant convection time}}{\text{vane passing period}} = \frac{fL}{V_c}\,, \tag{1}$$

where f is the vane passing frequency, L is the cooling hole length, and V_c the coolant velocity. If the reduced frequency is high, $\kappa \gg 1$, unsteady effects will dominate. If the reduced frequency is low, $\kappa \ll 1$, the flow can be considered *quasi-steady*, and the instantaneous unsteady flow is the same as a steady flow with the instantaneous boundary conditions.

Taking nominal values for the parameters representative of a 50 Hz large industrial gas turbine, the reduced frequency of a rotor cooling hole is of order $\kappa \approx 0.06$. This is a low value, and the hole is expected to behave quasi-steadily in this case. The quasi-steady assumption is also supported by measurements of steady and instantaneous unsteady aerodynamic fields. Bernsdorf et al. [13] observed quasi-steady behaviour at $\kappa = 0.03$, and Ligrani et al. [14] up to $\kappa \leq 0.16$.

The quasi-steady assumption simplifies modelling of the cooling hole flow, as existing steady characterisations can be applied separately at each instant in time. However, knowledge of the time-varying external boundary conditions is still required.

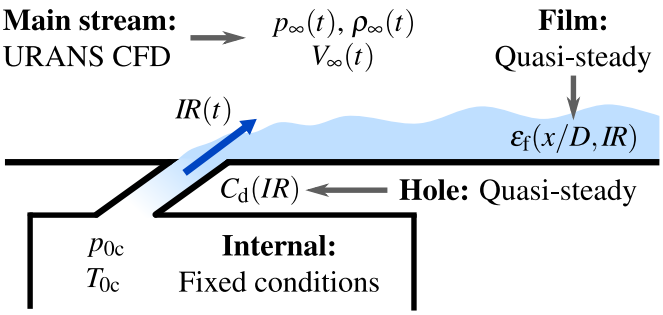

Fig. 2: Diagram of the unsteady film cooling modelling approach. Internal boundary conditions are fixed, main-stream boundary conditions are extracted from URANS computations, and the cooling hole is assumed to behave quasi-steadily.

Main-stream boundary conditions from URANS

Film cooling holes do not need to be resolved to predict blade row interactions; non-film-resolved simulations can capture the fluid-dynamic mechanisms causing unsteady main stream boundary conditions in the rotor. Therefore, blade row interaction is modelled using Unsteady Reynolds-averaged Navier–Stokes (URANS) simulations with the Spalart–Allmaras turbulence model, performed using TURBOSTREAM [15]. The solver, derived from the Denton code TBLOCK, has been extensively validated across a range of turbomachinery applications [15–17]. Appendix A contains full details of the computational method.

The case considered here is a proprietary geometry representative of a large industrial gas turbine. The computational domain is a one-eighth annulus sector including the first one-and-a-half stages of the high-pressure turbine. Referenced to isentropic mid-span upstream vane exit conditions, the Mach number is $M_{\text{ref}} \approx 0.7$, and the axial chord Reynolds number is $Re_{\text{ref}} \approx 4 \times 10^6$. There are two rows of film cooling holes at the leading edge, three on the suction surface, three on the pressure surface, and a trailing edge slot. The total coolant flow to the vane is 4.5% inlet mass flow. Film cooling is also present on the other aerofoil and endwall surfaces. Cooling holes are not meshed, and instead modelled using source patches imposing additional fluxes of mass, momentum and enthalpy. This simplified model is used *only* to capture the effects of coolant addition on the turbine aerodynamics, and not to predict cooling performance.

Instantaneous main-stream boundary conditions are extracted from the simulations at 5% of pitch away from the rotor blade surface, outside the region of influence of the cooling patches, and supplied as input to the hole response model.

Quasi-steady hole response model

The cooling hole operating point is fixed by the combination of momentum flux ratio, *IR*, and density ratio, *DR*, defined,

$$IR = \frac{\rho_c V_c^2}{\rho_\infty V_\infty^2} \ , \ \text{and,} \ \ DR = \frac{\rho_c}{\rho_\infty} \ , \tag{2}$$

where coolant properties are evaluated at the hole exit. The density ratio is directly set by the instantaneous coolant and main-stream boundary conditions (neglecting compressibility within the hole). The governing parameter for cooling hole aerodynamics is the momentum flux ratio, which requires knowledge of the unsteady coolant mass flow rate.

Constant values of plenum stagnation pressure and temperature are chosen as internal boundary conditions. For the purpose of this study, nominal values are assumed: a pressure margin of 3%, and a coolant to main-stream temperature ratio of 0.5, with respect to mass-averaged rotor-relative inlet conditions.

The discharge coefficient, C_d, is defined as the ratio of actual mass flow to ideal mass flow assuming a one-dimensional isentropic expansion from the coolant stagnation pressure to the main-stream static pressure. Rowbury et al. [18] presented a correlation for the discharge coefficient of cylindrical holes in terms of hole Reynolds number and momentum flux ratio under steady conditions. Taking the hole flow as quasi-steady, the instantaneous discharge coefficient and hole mass flow are given by evaluating the correlation at the instantaneous boundary conditions. A separate iterative calculation is required at each instant in time, because the momentum flux ratio itself is a function of the hole mass flow rate.

To summarise, the calculation steps for the hole response model are: (i) select coolant plenum conditions; (ii) extract unsteady main-stream conditions from URANS computations; (iii) calculate momentum flux ratio and discharge coefficient

at each instant in time using a steady correlation.

Film effectiveness modelling

A further assumption of quasi-steady film behaviour, i.e. that steady-state film effectiveness correlations can also be applied in unsteady flow, would furnish instantaneous cooling performance. However, there is no experimental or computational data available to confirm the assumption. In this paper, no attempt is made to model the unsteady film effectiveness, because of the extra assumptions involved. The design recommendations made are justified on aerodynamic computations and quasi-steady momentum flux ratio results, complemented by flat plate experimental measurements. The view of the authors is that high-fidelity computational modelling of the entire stage is required to predict quantitatively-accurate rotor film effectiveness.

NON-LINEARITY MEASUREMENTS

In this section, experimental measurements are used to confirm that, at fixed time-averaged boundary conditions, unsteady fluctuations on a non-linear hole characteristic change the time-averaged cooling performance. Film effectiveness data are presented as a real equivalent of the schematic in Fig. 1(b).

Experimental configuration

The aim of the experiment is to test the performance of cooling holes subject to main-stream unsteadiness. A new non-rotating, low-speed, and approximately isothermal rig was constructed to fulfil this aim with minimum complexity. Figure 3 displays a schematic of the apparatus. A high-level description of the set-up is given here, with further details contained in Appendix B.

The working section is attached to a blow-down wind tunnel exhausting to atmosphere. Coolant is pressurised separately and ducted to a plenum chamber which feeds a row of five cylindrical film cooling holes on a flat plate. A temperature difference is applied to the coolant flow using a heater mesh located in the plenum, and the downstream distribution of film effectiveness is obtained using a transient linear regression method on infra-red thermographic surface temperature data.

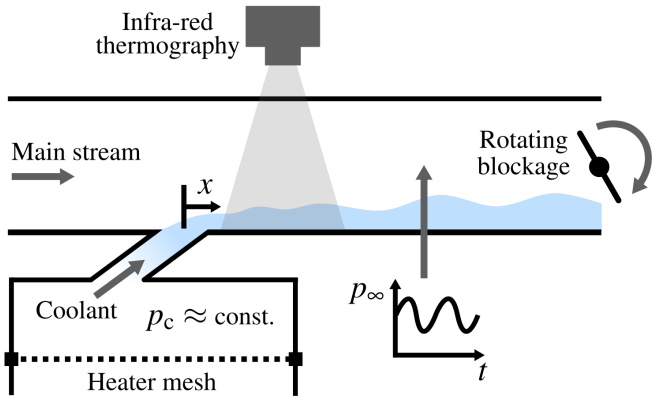

Fig. 3: Schematic of the experimental apparatus (not to scale). A rotating blockage at outlet oscillates the working-section exit area and hence main-stream static pressure.

As discussed in the Background section, a non-rotating rig must model blade row interaction unsteadiness in a simplified, idealised way. In the present experiment, a rotating blockage varies the exit area to produce a roughly sinusoidal oscillation in main-stream static pressure, after Ligrani et al. [14]. This is representative of potential field interactions present in the real turbine, but does not model wake turbulence. The method of forcing from downstream has the advantage that time-averaged boundary conditions can be precisely matched between steady and unsteady conditions, in order to test for non-linearity.

Non-dimensional geometry and boundary condition parameters for the film cooling tests are listed in Table 1. As the rig is approximately isothermal, the density ratio is close to unity, $DR \approx 1$. The momentum flux ratio is a suitable scaling parameter for film cooling aerodynamics across different density ratios [19]. No main-stream turbulence is introduced and the turbulence intensity remains below 1% in all tests. Unsteady forcing is characterised by a main-stream reduced frequency and non-dimensional amplitude. The main-stream reduced frequency, κ_∞, is defined,

$$\kappa_\infty = \frac{fD}{V_\infty} \,, \tag{3}$$

similar to the reduced frequency in Eqn. (1), but using a main-stream convective time scale. Defined in such a way, it is independent of the cooling hole operating point. The mean-to-peak amplitude of static pressure fluctuation, $\widetilde{p_\infty}$, is scaled on the time-averaged main-stream dynamic head to form a non-dimensional amplitude Ψ, according to,

$$\Psi = \frac{\widetilde{p_\infty}}{p_{0\infty} - p_\infty} \,. \tag{4}$$

Table 1: Non-dimensional parameters for flat-plate film cooling tests. Boundary-layer properties are measured at $x/D = -10$. All parameters excluding Mach number, temperature ratio, and turbulence intensity are matched to turbine conditions.

Inclination angle,	$\alpha = 30^\circ$
Pitch-to-diameter ratio,	$P/D = 4$
Length-to-diameter ratio,	$L/D = 6$
Mach number,	$M_\infty \to 0$
Reynolds number,	$Re_\infty = 15\,000$
Turbulence intensity,	$Tu_\infty < 1\%$
Boundary layer displacement thickness,	$\delta^*/D = 0.074$
Boundary layer shape factor,	$H = 1.41$
Temperature ratio,	$T_{0c}/T_{0\infty} = 1.1$
Momentum flux ratio,	$IR = 0.2$ to 2.0
Reduced frequency,	$\kappa_\infty = 0.005$
Pressure fluctuation amplitude,	$\Psi = 0.0,\ 0.4$

Values of $\kappa_\infty = 0.005$ and $\Psi = 0.4$ are chosen as representative based on results from the turbine stage computations, presented later in the paper.

Experimental results

The results are first presented as streamwise distributions of laterally area-averaged film effectiveness in Fig. 4, the shaded bands denoting confidence intervals based on 18 repeated measurements. The holes are tested at four time-averaged momentum flux ratios, with and without main-stream forcing at $\Psi = 0.4$.

At low momentum flux ratio, $IR = 0.2$, the effect of unsteadiness is significant, with with main-stream static pressure oscillations reducing film effectiveness at all streamwise locations by between 0.03 and 0.06, or between 26% and 31%. However, this behaviour is not replicated at high momentum flux ratios, $IR \geq 1.0$, where the steady and unsteady film effectiveness distributions differ by less than 0.01. For these cases, the root-mean-square changes in film effectiveness are 0.003 and 0.005, while the root-mean-square confidence intervals are 0.003 and 0.007. At high momentum flux ratio, the effect of unsteadiness is small enough to be indistinguishable from the measurement uncertainty. At an intermediate momentum flux ratio, $IR = 0.6$, unsteadiness increases film effectiveness by approximately 0.009. The effect is distinguishable from but of the same order as the measurement uncertainty. An unsteadiness benefit has been previously reported by Seo et al. [10].

These trends in film effectiveness can be explained with reference to the film effectiveness characteristic in Fig. 5. This shows the local laterally-averaged film effectiveness under steady boundary conditions, at $x/D = 8$, plotted as a function of momentum flux ratio. In the low reduced frequency limit, the film effectiveness will follow this line during unsteady excursions. The steady operating points corresponding to the solid lines in Fig. 4 are shown by the filled circles at various

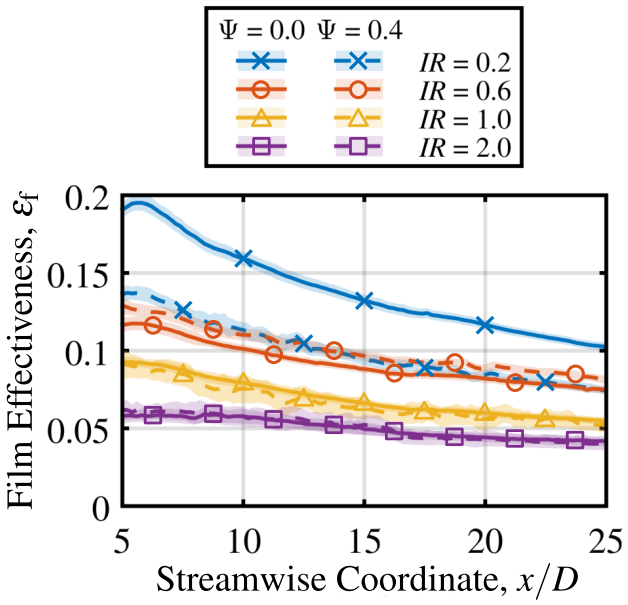

Fig. 4: Measured streamwise distributions of laterally-averaged film effectiveness, with and without unsteadiness. At low momentum flux ratio, $IR = 0.2$, unsteadiness reduces film effectiveness by up to 0.06 or 31%; at high momentum flux ratio, $IR \geq 0.6$, the effect on film effectiveness is small.

locations on the characteristic. The time-averaged unsteady film effectiveness results, corresponding to the dashed lines in Fig. 4, are shown with open circles.

When the coolant is attached to the surface at low momentum flux ratio, $IR = 0.2$, the hole responds non-linearly to fluctuations about the time-averaged boundary condition. A reduction in momentum flux ratio reduces the coolant mass flow, while an increase in momentum flux ratio increases coolant lift-off. Both of these act to reduce instantaneous film effectiveness: at $x/D = 8$, the time-averaged effect is a 30% reduction. Indeed, about a peak on the characteristic, which is by definition non-linear, *any* unsteady movement away from the mean leads to a reduction in time-averaged film effectiveness.

As the momentum flux ratio increases, coolant lift-off increases, and the film effectiveness characteristic flattens, i.e. becomes less sensitive to momentum flux ratio perturbations. For the time-averaged operating points at $IR \geq 0.6$, the excursions in film effectiveness about the mean are approximately linear, so positive and negative movements in momentum flux ratio balance each other out, and the time-averaged effect of unsteadiness is small, changing the local film effectiveness by less than $\pm 5\%$. The marginal increase in effectiveness at $IR = 0.6$ is attributed to slight positive curvature, i.e. non-linearity, of the characteristic at that operating point.

Discussion of non-linearity measurements

The measurement data show that, at constant time-averaged boundary condition, unsteadiness has a small effect in linear regions of the hole characteristic, and a large effect at the non-linear peak of the characteristic. This motivates the following design recommendation: in an unsteady flow, the hole geometry and time-averaged operating point should be selected such that the hole characteristic is linear over the anticipated range of fluctuation in boundary condition.

The results suggest that conventional cylindrical cooling holes are robust to unsteadiness in this respect. At momentum flux ratios representative of turbine conditions, say $IR \geq 0.6$, where the coolant is lifted-off, the hole characteristic is approximately linear and so non-linear unsteady effects are small. In general, the characteristic of the particular film cooling geometry of interest should be considered, which may not be so benign.

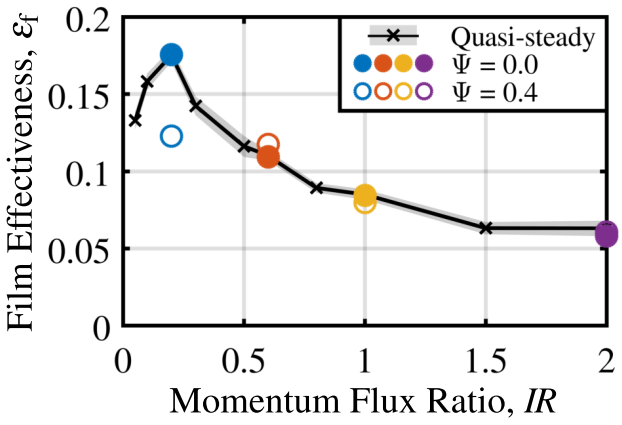

Fig. 5: Measured film effectiveness characteristic at $x/D = 8$, with steady and time-averaged operating points shown as circles. Movement on non-linear characteristic about $IR = 0.2$ causes a reduction in local film effectiveness of 30%, while operating points in linear regions are less affected.

MECHANISMS OF BLADE ROW INTERACTION

In this section, the blade row interaction mechanisms generating main-stream unsteadiness are characterised by interrogation of URANS computations. Rotor incidence, wake interaction, and potential field interaction are discussed in turn.

Rotor incidence

The flow angle leaving the upstream stator is non-uniform, as shown by the pitchwise profile of rotor-relative yaw angle in Fig. 6, upper. This is not seen by the rotor in a steady mixing-plane computation. There is a trough of localised negative incidence, down to $\alpha_{\text{rel}} = 20^\circ$, within the wake at 50% vane pitch, and also a long-wavelength variation in yaw angle from 36° to 48° due to the vane potential field. The variation in blade leading edge flow field as it rotates through the non-uniform flow angle is shown in Fig. 6, lower. Instantaneous contours of static pressure are shown for the maximum incidence, Fig. 6(a), and minimum incidence, Fig. 6(b), positions. The static pressure is plotted as a pressure coefficient referenced to (time-averaged) isentropic rotor exit conditions,

$$C_p = \frac{p_{0\text{ref}} - p}{p_{0\text{ref}} - p_{\text{ref}}} \ . \tag{5}$$

The nominal showerhead position is marked with a blue dot, while the stagnation point location on the leading edge circle is marked in black. The stagnation point crosses the showerhead during the vane passing cycle, varying from $+8^\circ$ to -12° relative to the showerhead position. If the designer were to place a cooling hole at the blue dot, it would respond non-linearly to stagnation point movement, due to the discontinuity as coolant is alternately and exclusively directed to pressure and suction sides.

Johnson et al. [20] measured overall effectiveness for a single cooling hole on a leading edge model with an oscillating stagnation point: a decrease of up to 25% due to unsteadiness was found, confirming that the response is non-linear. An amplitude of oscillation of $\pm 5^\circ$ was estimated from a nominal wake velocity deficit and velocity triangle arguments. A similar analysis for the present stage predicts the expected incidence oscillation to within 1°. The results of the current study corroborate the existence of stagnation point oscillations in a real turbine, and suggest the amplitude can be directly inferred from the upstream non-uniformity.

Wake interaction

The ‘negative jet’ is a blade row interaction mechanism well-known in the literature [21]. It will be shown that the negative jet creates main-stream velocity perturbations, altering the instantaneous cooling hole operating point. The negative jet also causes vane coolant to migrate across the rotor passage and affect time-averaged film effectiveness.

Perturbation values for a flow property can be defined as the instantaneous unsteady minus the time-averaged value. These perturbations with respect to the time average will be denoted with a prime. Figure 7 is an instantaneous snapshot of the velocity perturbation on a mid-span streamsurface. The contours indicate the magnitude of the perturbation, normalised by the isentropic rotor exit reference velocity, and vectors are also plotted to illustrate the associated direction. A classical negative jet exists within the wake, with vectors acting towards the suction side. The magnitude of the velocity perturbations is up to $\pm 15\%$ of the reference velocity, a non-negligible fraction of the time-averaged main-stream velocities at cooling hole

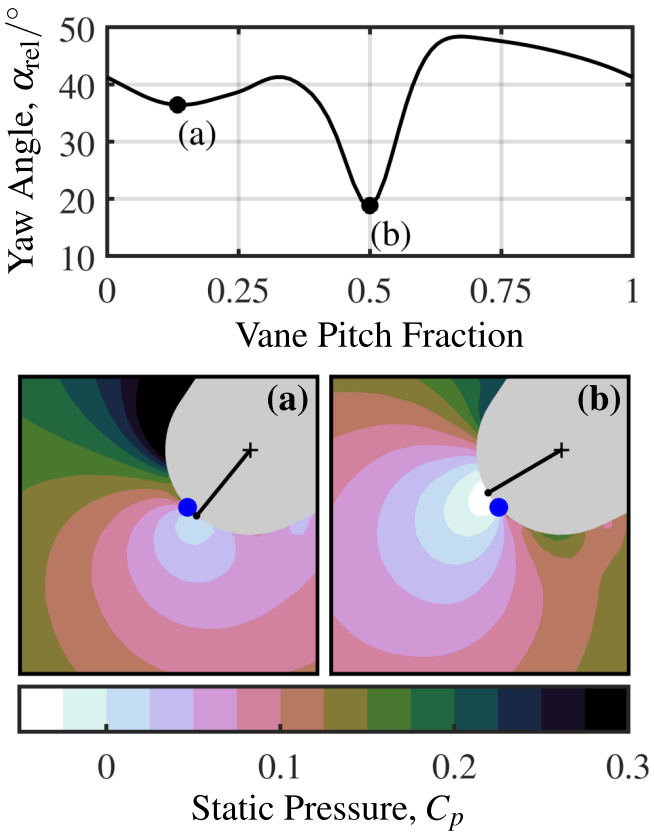

Fig. 6: **Upper:** pitchwise profile of upstream vane exit rotor-relative yaw angle. **Lower:** contours of instantaneous static pressure near rotor leading edge at **(a)** maximum incidence, **(b)** minimum incidence, showerhead location marked with a blue dot. The stagnation point moves across the showerhead during a vane passing cycle, from $+8^\circ$ to -12° on the leading edge circle.

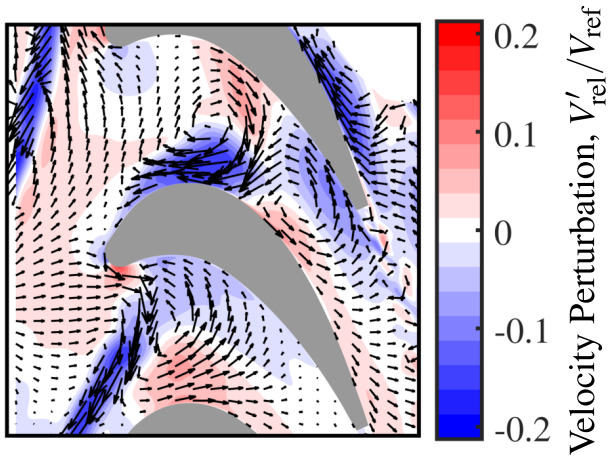

Fig. 7: Contours of instantaneous relative velocity magnitude perturbation, normalised by isentropic rotor exit velocity, at rotor mid-span. Arrows show direction of the velocity perturbation. A 'negative jet' acts towards the suction side, perturbing the main-stream velocity by $\pm 15\%$ reference velocity.

locations of 20% to 75% reference velocity. This affects the instantaneous cooling hole operating point via the denominator of momentum flux ratio in Eqns. (2). If the hole is operating on a non-linear characteristic, this will alter the time-averaged performance.

If the upstream vane has film cooling, as is the case for the high-pressure turbine rotor, wake interaction also affects the time-averaged temperature field within the rotor passage. This is a kinematic effect, where cold fluid within the vane wake is carried towards the suction side by the negative jet. The effect is quantified using contours of time-averaged relative stagnation temperature at rotor mid-span in Fig. 8. The temperature is plotted as an effectiveness with respect to the mass-averaged rotor inlet temperature and blade coolant temperatures,

$$\Theta = \frac{T_{0\infty,\mathrm{rel}} - T_{0,\mathrm{rel}}}{T_{0\infty,\mathrm{rel}} - T_{0\mathrm{c},\mathrm{rel}}} \ , \tag{6}$$

such that $\Theta = 0$ corresponds to the nominal main-stream temperature in a steady computation, and $\Theta = 1$ corresponds to full cooling on the rotor surface.

Predictions from a steady, mixing-plane computation are shown in Fig. 8(a). The film cooling can be identified as the dark red areas around the blade. Away from the films the stagnation temperature is $\Theta \approx 0$ throughout the rotor passage as expected. The prediction from an unsteady computation is shown in Fig. 8(b), with variations in relative stagnation temperature across the passage equivalent to ± 0.03 in blade film effectiveness. This is $\pm 15\%$ of a typical design target of $\varepsilon_\mathrm{f} \approx 0.2$. The positive area near the suction side, and negative area near the pressure side, are consistent with the established behaviour of cold wake fluid (positive effectiveness) migrating with the negative jet. However, close to the suction side, the effectiveness reduces again, indicating the true kinematics of the flow are more complex than a one-dimensional cross-stream description. A trend of reduced pressure-side effectiveness, and no change or an increase in suction-side effectiveness, is observed in the available rotating-stage measurements with cooled upstream vanes [2, 11].

With a uniform upstream stagnation temperature, as in Fig. 8(a), using laboratory flat plate or cascade test data, the film effectiveness can be scaled to engine conditions by matching the non-dimensional boundary conditions, such as momentum flux ratio. The non-uniform stagnation temperature in Fig. 8(b) means that the adiabatic wall temperature of the uncooled rotor is not known a-priori, and laboratory film effectiveness tests do not scale to the correct cooled turbine adiabatic wall temperature. This result makes explicit the fact that a credible design prediction of rotor film cooling performance must account for migration of vane coolant due to blade row interaction.

Finally, another effect of wake interaction is the elevation of main-stream turbulence intensity as the wake passes. For a fixed momentum flux ratio, the effect of wake turbulence may be adequately modelled using just a time-averaged turbulence intensity if the film effectiveness responds linearly to a change in turbulence intensity. There is no evidence in the literature to suggest a non-linear response. Saumweber et al. [6] found that the effect of unsteady wakes and elevated steady main-stream turbulence were similar, which suggests linear behaviour. A confirmation of the effect would require fully-resolved film modelling.

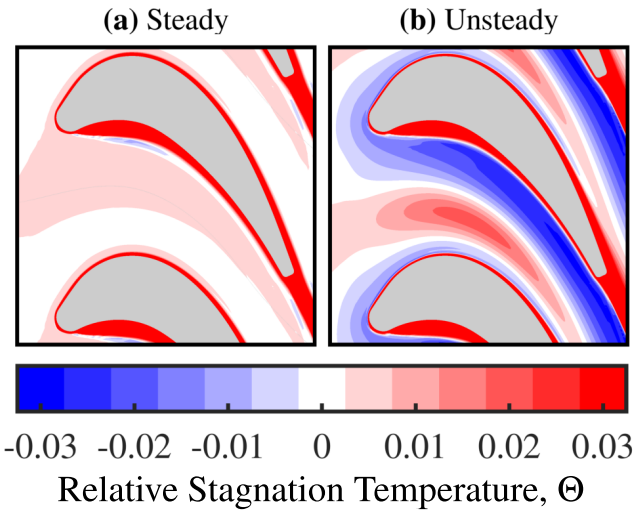

Fig. 8: Contours of time-averaged relative stagnation temperature at rotor mid-span, plotted as effectiveness referenced to rotor inlet mass-averaged and blade coolant temperatures, **(a)** steady, and **(b)** unsteady simulations. With wake interaction, redistribution of vane coolant alters effectiveness by ± 0.03.

Potential field interaction

The loading and blockage of a vane row creates an inviscid flow non-uniformity, or 'potential field'. To a close approximation, the distortion is 'frozen' to the stator row and hence rotates circumferentially at blade speed relative to the rotor.

Unsteady pressure field

Figure 9 shows four snapshots of the unsteady static pressure perturbation at rotor mid-span during the upstream vane passing. The pressure coefficient is defined using isentropic rotor exit conditions as the reference, Eqn. (5). The boundary of the upstream vane wake is shown using a line contour of zero entropy perturbation. The frozen potential field originating from the upstream vane can be identified as a circumferential distortion of $\pm 10\%$ reference dynamic head moving downwards at the left edge of the frame, wavelength 2.4 rotor pitches. The potential field of the downstream vane, wavelength 1.5 rotor pitches, is not so distinct, with small pressure perturbations of less than $\pm 3\%$ reference dynamic head at the right edge of the frame. Because the pitch of the downstream vane is 63% that of the upstream vane, the downstream potential field decays rapidly, to a negligible level before reaching the rotor. The upstream vane potential field is imposed at the rotor leading edge and causes surface static pressure perturbations of $\pm 10\%$ reference dynamic head. Pressure fluctuations are also present throughout the rotor passage, including locations remote from the leading edge, of the same order as the cooling hole pressure drops of 10% to 60% reference dynamic head. This will produce unsteadiness in hole operating point.

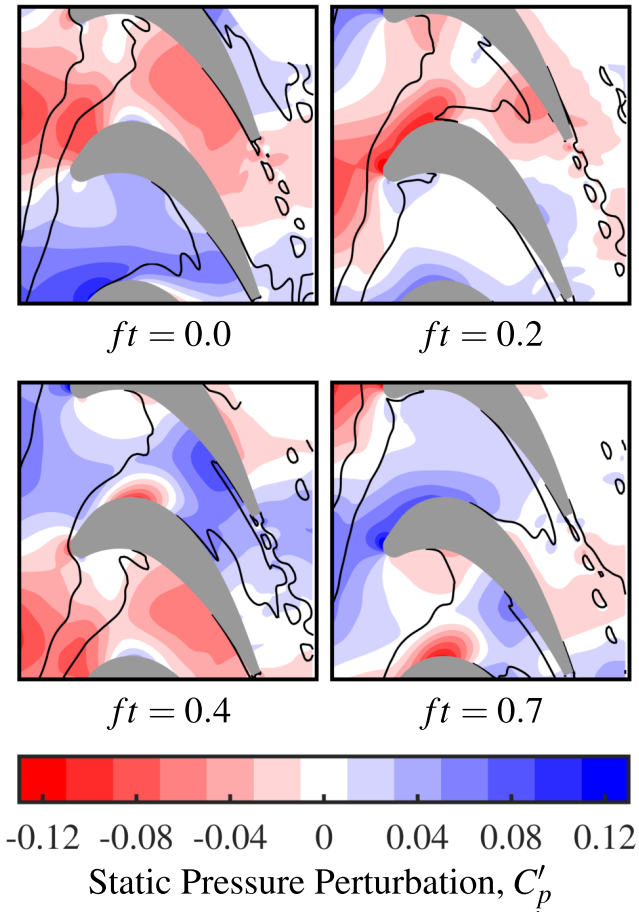

Fig. 9: Instantaneous static pressure perturbation contours at rotor mid-span at four snapshots during upstream vane passing, wake marked with entropy perturbation line contours. The rotor main-stream static pressure fluctuates by $\pm 10\%$ isentropic rotor exit dynamic head.

Modelling potential field propagation

The amplitude of non-uniformity associated with the potential field of an isolated row of vanes decays exponentially, on a length scale proportional to the vane pitch. However, it is evident from Fig. 9 that the pressure fluctuations originating from the upstream vanes do not behave in this way when interacting with the rotor: the disturbance is in fact amplified within the passage. Kachel and Denton [22] identified one-dimensional pressure waves in measurements and calculations of a multi-stage, low-speed turbine rig. These were asserted to be the dominant cause of static pressure fluctuations on the rotor pressure side. In this paper, a simple model is used to extend the existing understanding of propagating potential field interaction.

The one-dimensional, compressible, unsteady Euler equations are solved over a straight contracting duct, modelling the rotor passage along a medial axis from inlet to throat. The area variation of the duct with streamwise distance, ξ, is determined from the radius of the medial circle, $h(\xi)$ as shown in Fig. 10. A finite-volume spatial discretisation is used, with a second order accurate central difference formulation. The equations are integrated using the SCREE scheme by Denton [23], with dual time stepping used to recover second-order time accuracy. Time-resolved boundary conditions for inlet relative stagnation temperature and pressure, and throat static pressure, are extracted from the unsteady three-

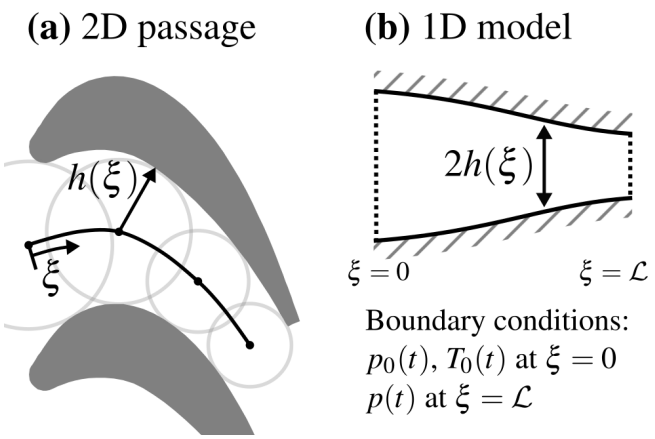

Fig. 10: Reduction of two-dimensional rotor passage **(a)** to one-dimensional model **(b)**. The passage is straightened about the medial axis into a duct, with half-height equal to the medial circle radius. Time-resolved boundary conditions extracted from URANS computations are imposed at the inlet and throat.

dimensional simulations. The quantity of interest is the mean-to-peak fluctuation amplitude of the static pressure on the rotor surface.

For each location on the medial axis ξ, the pressure fluctuation amplitude is extracted from the unsteady three-dimensional simulation at points where the medial circle touches the rotor pressure and suction sides, and plotted in Fig. 11. Traces are shown for two cases: the *Datum* configuration with a cooled upstream vane, and a *Potential* configuration with no vane wakes or cooling. These cases are described in more detail in the final part of this paper. Here, we note that the two cases produce differing amplitudes of surface pressure fluctuation, by up to 75%, indicating that the unsteady pressure field is strongly influenced by wake interaction, in addition to potential field interaction. This can also be inferred from Fig. 9, say, at $ft = 0.4$, with a red region of increased static pressure on the suction side within the wake. The one-dimensional model is not expected to predict wake interaction, so is compared with the *Potential* case. On the pressure side, the qualitative behaviour is well-captured by the model, and the quantitative agreement is within 20% over most of the blade surface. This suggests that the propagating potential field interaction can be approximately modelled as one-dimensional pressure waves, supporting the assertion of Kachel and Denton [22]. On the suction side, the model produces the correct qualitative behaviour for the rear 50% of medial axis distance, but the model and three-dimensional simulation diverge towards the rotor leading edge, with an error of up to 40%. This is because the one-dimensional model does not capture two-dimensional streamline curvature effects, most significantly within the vane wake.

Summary of interaction mechanisms

This section has identified the blade row interaction mechanisms affecting rotor film cooling in a representative large industrial gas turbine. These mechanisms are listed in Table 2, grouped into inviscid, potential effects, and wake effects.

Two mechanisms alter the time-averaged boundary conditions, resulting in a change in film effectiveness of type Fig. 1(a). These are: vane coolant migration, by redistributing the main-stream stagnation temperature; and vane wakes,

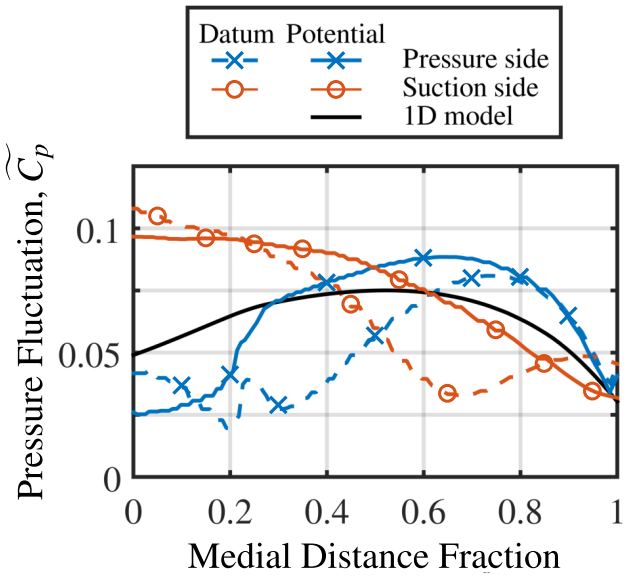

Fig. 11: Comparison of one-dimensional rotor passage model with three-dimensional simulation results. In the potential case, the mean-to-peak static pressure fluctuation amplitude agrees qualitatively, excluding front 50% of the suction side.

by increasing the main-stream turbulence intensity. The other mechanisms in Table 2 affect the instantaneous flow, causing unsteady excursions in cooling hole operating point. If the hole characteristic is non-linear, this results in a change in film effectiveness of type Fig. 1(b).

Table 2: Summary of blade row interaction mechanisms affecting rotor film cooling, * denotes a time-averaged effect.

Potential	Frozen vane pressure field
	One-dimensional pressure waves
Wake	Stagnation point movement
	Negative-jet velocity perturbations
	Curvature pressure perturbations
	Vane coolant migration*
	Main-stream turbulence*

HOLE RESPONSE MODELLING

In this section, the quasi-steady hole response model is used to predict unsteady excursions in momentum flux ratio of rotor cooling holes. Four hole locations on the rotor mid-span streamsurface are chosen, shown on Fig. 14, representative

of the cooling configuration in a large industrial gas turbine. Results are presented for steady and unsteady simulations, to quantify the total effect of blade row interaction. Results are also presented for a series of modified upstream vanes, to assess the relative influence of wake and potential field interactions.

Time-averaged comparison

Steady simulations, with a mixing plane between blade rows, are typically used in the design process. A mixing plane uses a circumferential averaging procedure to enforce steady, uniform flow entering each row. To assess the effect of this approximation on determination of time-averaged momentum flux ratio, the *Datum* unsteady case, as analysed in the previous part of this paper, is compared to a *Steady* case with mixing planes. A further *Linear* case is a steady calculation of momentum flux ratio using the time-averaged unsteady *Datum* boundary conditions, i.e. what would be expected from a linear hole response.

The changes in time-averaged momentum flux ratio in the *Datum* and *Linear* cases with respect to the *Steady* case are shown in Fig. 12. In the *Datum* case, blade row interaction modifies the time-averaged momentum flux ratio by up to $+6.3\%$ at the suction side hole. The *Linear* case does not reproduce the *Datum* values, in error by up to 10% at the showerhead hole. This shows that the momentum flux ratio responds non-linearly to unsteadiness, which cannot be accounted for in design by simply using main-stream boundary conditions taken from a time-averaged unsteady computation.

Modified upstream vanes

From the complete list of blade row interaction mechanisms identified in Table 2, it is of interest to quantify the relative influence of each mechanism. This directs the designer towards the turbine aerodynamic adjustments that would best mitigate blade row interaction effects.

A series of numerical experiments, where the upstream vane is modified, is used to vary the relative strength of wake and potential field interactions and distinguish their individual effects. The configuration of the computational model in each of these cases is listed in Table 3. The *Datum* case is representative, with a cooled vane. The *Uncooled* case removes the

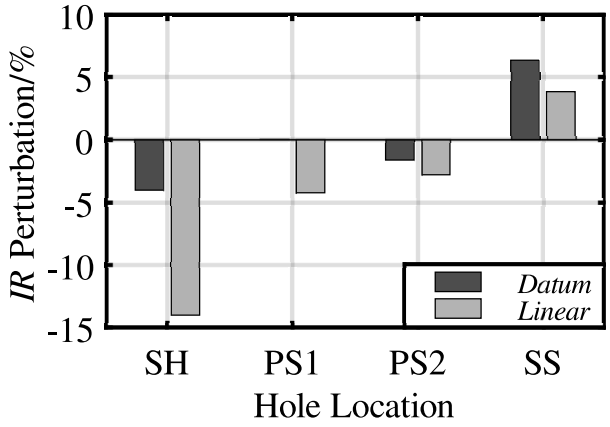

Fig. 12: Change in time-averaged momentum flux ratio of rotor cooling holes predicted by quasi-steady model, with respect to *Steady* case. The momentum flux ratio responds non-linearly to unsteadiness.

vane film and trailing edge cooling, but retains the viscous wake. Finally, the *Potential* case uses a sharp trailing edge and an inviscid wall on the vane surface to eliminate the wake, leaving only a potential field. With the modified vanes, the upstream vane is restaggered to correct for changes in deviation; the vane exit flow angles of each case then match to within 0.2°. Also, the downstream blade and vane are restaggered closed to maintain the same pressure drop with reduced coolant mass flow. The vane exit Mach number, a proxy for loading and hence potential field, is held constant to within 2% across the three cases.

A comparison of the exit flow non-uniformity for the modified vanes is shown in Fig. 13. Pitchwise profiles of rotor-relative flow angle and static pressure coefficient are plotted, time-averaged in the absolute frame, for the upstream vane exit mid-span. Figure 13(a) shows that the flow angle deficit within the wake reduces from 25° to 10° as the coolant is removed in the *Uncooled* case, and is then eliminated when the wake is removed in the *Potential* case. The inviscid flow angle variation of $\pm 6^\circ$ is common to all cases. The profiles of static pressure in Fig 13(b) agree closely, to within $\pm 1.5\%$ reference dynamic head, confirming that the potential field interactions are comparable.

Unsteady comparison

Quasi-steady model predictions of unsteady momentum flux ratio for each of four cooling hole locations on the rotor blade are displayed in Fig. 14. Traces are shown for all four cases in Table 3. In the *Datum* case, each hole experiences oscillations in momentum flux ratio of not less than $\pm 30\%$, up to $+140\%$ for the leading edge showerhead in Fig. 14(a). It cannot be assumed in general that a cooling hole will behave linearly over such a large movement on the hole characteristic, and non-linear effects may therefore play a role.

If potential field interaction was the only driver of rotor film cooling unsteadiness, the traces for each modified vane would be identical, because the vane loading is held constant. This is approximately the case for some parts of the vane passing cycle, for example $0.4 \leq ft \leq 0.8$ in Fig. 14(a) and $0.2 \leq ft \leq 0.5$ in Fig. 14(c). At these times, the wake is away from the cooling hole, and does not affect the operating point, leaving only the potential field interaction that is common to all cases.

However, for the part of the vane passing cycle where the wake is present, it has a significant additional effect on the momentum flux ratio by changing the main-stream velocity. On the pressure side, Fig. 14(c), the negative jet reduces main-stream velocity ahead of the wake, increasing momentum flux ratio. After the wake passes over the cooling hole at $ft = 0.8$, the main-stream velocity increases and momentum flux ratio reduces. On the suction side, the converse happens, consistent

Table 3: Analysis cases for hole response modelling.

	Mixing plane	Coolant	Wake
Steady	✓	✓	✓
Datum		✓	✓
Uncooled			✓
Potential			

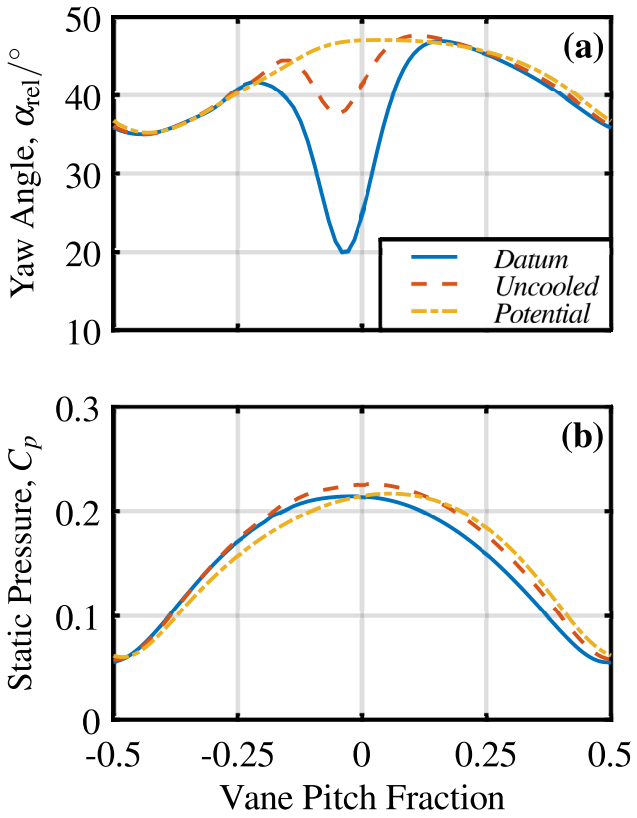

Fig. 13: Pitchwise profiles of **(a)** rotor-relative yaw angle and **(b)** static pressure, at vane exit for the modified upstream vanes. The strength of the negative jet is varied at constant potential field.

with the negative jet kinematics in Fig. 7. The perturbation associated with the wake is larger than the potential field. The result is that not modelling wake interactions reduces momentum flux ratio excursions, for example for the suction side hole in Fig. 14(d), from $\pm 32\%$ to $\pm 8\%$. For holes on the pressure side, where negative-jet velocity perturbations are relatively smaller (Fig. 7), the wake effect is greater than the potential by a factor of 2. For holes on the suction side and showerhead, regions of larger negative-jet perturbations, the wake effect is greater by up to a factor of 5.

The wake effect is greater in the *Datum* case than in the *Uncooled* case, shown by comparing the departure of these cases with respect to the *Steady* case, most clearly in Figs. 14(a) and 14(d). This is because the wake negative jet is augmented by the addition of vane coolant. The timing of the wake impact with respect to potential field interaction also affects the instantaneous momentum flux ratio. For example, in Fig. 14(b), the wake arrives during a trough in *Potential* momentum flux ratio at $ft = 0.35$, and in Fig. 14(a), at the peak at $ft = 0.2$.

CONCLUSIONS AND RECOMMENDATIONS

Conclusions

Based on the results presented in this paper, the following conclusions are drawn:

1. With an unsteady main-stream, a cooling hole operating on a non-linear characteristic does not produce the film ef-

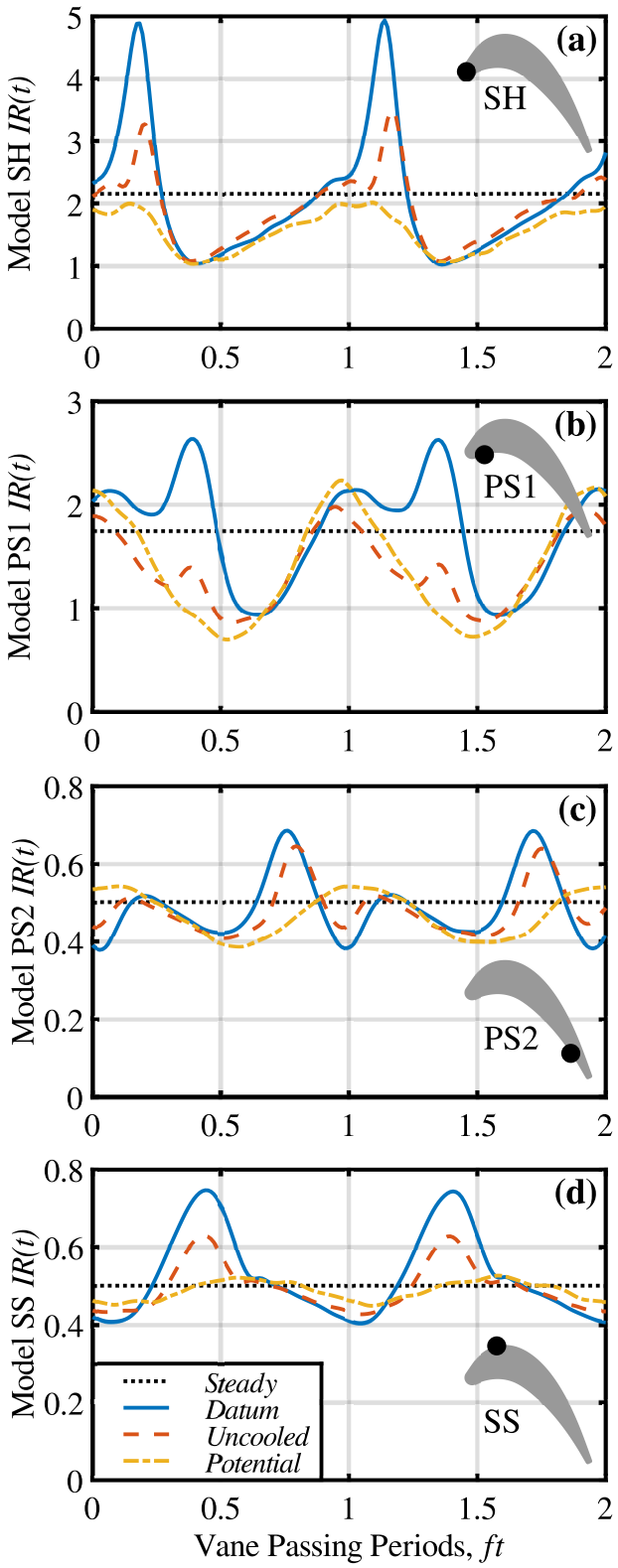

Fig. 14: Instantaneous momentum flux ratio of rotor cooling holes predicted by quasi-steady model: **(a)** showerhead, SH; **(b)** front pressure side, PS1; **(c)** rear pressure side, PS2; and **(d)** suction side, SS.

fectiveness expected from the time-averaged boundary condition. For cylindrical holes at low momentum flux ratio, representative unsteadiness was measured to reduce laterally-averaged film effectiveness by up to 0.06 or 31%.

2. In a turbine stage, the rotor leading edge stagnation point oscillates in response to the non-uniform upstream vane exit flow angle, by a predicted $\pm 10^{\circ}$ on the leading edge circle in the studied turbine. The magnitude of oscillation is set by the upstream flow non-uniformity.

3. With a cooled upstream vane, transport of coolant across the rotor passage by the wake negative jet affects the time-averaged rotor passage temperature field, by up to ± 0.03 effectiveness in the studied turbine.

4. The instantaneous momentum flux ratio of rotor cooling holes fluctuates in response to both wake and potential field interaction. In the studied turbine, wake interaction produces perturbations greater than potential field interaction by a factor of 2 to 5. The momentum flux ratio of all holes is observed to fluctuate by at least $\pm 30\%$, and up to $+140\%$ for the leading edge showerhead.

Recommendations

The conclusions lead to the following recommendations for the design of film cooling in the unsteady turbine environment:

1. The designer should choose a cooling hole characteristic and nominal time-averaged operating point which behaves linearly over the expected unsteady excursions, which may be found using a quasi-steady model;

2. Leading-edge cooling holes should be placed outside of the unsteady motion range of the stagnation point;

3. A credible design prediction of rotor film cooling performance must account for the redistribution of vane coolant due to blade row interaction.

Achnowledgements

The authors would like to thank Mitsubishi Heavy Industries for funding this project, and, specifically, Dr. S. Aoki, Dr. S. Uchida, Dr. E. Ito, Mr. H. Kitagawa, and Mr. Y. Kimura for their interest and support. The authors are also grateful for the comments and suggestions of Dr. N. Atkins, and our other colleagues at the Whittle Laboratory.

APPENDIX A: COMPUTATIONAL DETAILS

The URANS simulations used to provide input to the quasi-steady hole response model are described here. The computations are performed using TURBOSTREAM, a GPU-accelerated, multi-block structured URANS solver [15]. The spatial discretisation is second-order accurate finite-volume, with single-step explicit time marching and three levels of multigrid. The temporal discretisation is second-order accurate using Jameson's dual time stepping method; 72 time-accurate steps are used per rotor blade passing period.

The Spalart–Allmaras turbulence model is used, assuming fully-turbulent boundary layers. Due to the high Reynolds number of the studied turbine, $Re_{\text{ref}} \approx 4 \times 10^6$, at the design operating condition flow separation and transition effects are

not significant. Therefore, a relatively simple turbulence model calibrated for attached boundary layers and free shear flows is expected to perform adequately.

The domain comprises the first one-and-a-half high-pressure turbine stages of a large industrial gas turbine: an upstream stator, rotor, and downstream stator. At the inlet plane, six axial chords upstream of the stage, experimentally-measured radial profiles of stagnation temperature, stagnation pressure and flow angles are imposed. An exit static pressure distribution, six axial chords downstream, is derived from a measured static pressure on the hub assuming simple radial equilibrium. At solid boundaries wall functions are used, assuming fully-turbulent boundary layers, with a typical non-dimensional wall resolution of $\Delta y^+ \approx 30$. Surface patches with additional fluxes of mass, momentum and enthalpy are used to approximate the impact of coolant on the turbine aerodynamics (the resultant surface temperature distributions are not used). A one-eighth sector of the annulus was simulated to model the correct vane:blade:vane count ratio. A multi-block structured mesh was generated for each of the three rows using the commercial software NUMECA AUTOGRID 5, with an 'O-H' topology in each passage. The mesh has 89 spanwise points, with 17 in the rotor tip gap, and an overall density of approximately 1.5 million cells per passage. The single-passage meshes are duplicated in the circumferential direction to give a one-eighth annulus sector with 33 million nodes.

The computations are started from a converged steady solution, run for two sector periods to flush transients, and data is output over one further sector period. An entire simulation requires nine hours of wall-clock time running on four NVIDIA P100 graphical processing units.

APPENDIX B: EXPERIMENTAL DETAILS

The main-stream stagnation and static pressure are measured using a Pitot tube and wall tapping respectively, connected to a pressure scanner. Ambient pressure is measured using a digital barometer. Thermocouples are used to measure the main-stream and coolant temperatures. The coolant mass flow is measured using an ISO 5167 orifice plate. These data are sufficient to determine the Reynolds number, with an uncertainty of $\pm 0.9\%$, and momentum flux ratio, with an uncertainty of $\pm 2.0\%$. During testing, the nominal, time-averaged Reynolds number and momentum flux ratio are controlled to within $\pm 0.2\%$ and $\pm 1.0\%$ respectively.

Kulite fast-response pressure transducers are used to measure the main-stream and plenum static pressures. Accuracy is limited by in-situ calibration against steady pressure data, giving an uncertainty in normalised main-stream pressure fluctuation amplitude of $\pm 1.8\%$.

A low-conductivity foam plate is mounted downstream of the cooling holes and painted black. A FLIR SC7300L infrared camera is used to measure instantaneous surface temperature data. A calibration gradient is found through fitting to images of a thermocouple-instrumented plate, and a per-pixel offset is calculated at the start of each test using an image with no coolant flow. A step in coolant temperature of 40 K is applied using a mesh heater, and the impulse response method of Oldfield [24] is used to evaluate instantaneous heat flux from the surface temperature history. After O'Dowd et al. [25], linear regression of instantaneous heat flux against temperature is performed at each pixel: the gradient is the heat transfer coefficient, and the extrapolated intercept the adiabatic wall temperature, which is non-dimensionalised to yield film effectiveness. A pessimistic a-priori error analysis yields an uncertainty of ± 0.015 in film effectiveness. Averaging over 20

repeated tests, discarding two outliers, the precision error or confidence interval in mean measured effectiveness is reduced to between ± 0.003 and ± 0.01 depending on the flow condition.

NOMENCLATURE

Latin

h	One-dimensional duct height [m], Fig. 10
DR	Hole density ratio [-], Eqns. (2)
IR	Hole momentum flux ratio [-], Eqns. (2)
C_p	Static pressure coefficient [-], Eqn. (5)
D	Cooling hole diameter [m]
f	Upstream vane passing frequency [Hz]
L	Cooling hole length [m]
$\dot{m}$	Mass flow rate [$\mathrm{kg\,s^{-1}}$]
p	Pressure [Pa]
t	Time [s]
T	Temperature [K]
V	Velocity [$\mathrm{m\,s^{-1}}$]
x	Axial or streamwise coordinate [m]

Greek

α	Flow yaw angle; hole inclination angle [$^\circ$]
γ	Ratio of specific heats [-]
ε_f	Film effectiveness, laterally-averaged [-]
Θ	Normalised temperature [-], Eqn. (6)
κ	Reduced frequency [-], Eqns. (1) or (3)
ξ	Medial axis distance [m], Fig. 10
ρ	Density [$\mathrm{kg\,m^{-3}}$]
Ψ	Pressure fluctuation amplitude [-], Eqn. (4)

Subscripts and accents

0	Stagnation conditions
∞	Main-stream conditions
c	Coolant conditions
rel	Rotor-relative frame
ref	Isentropic mid-span exit conditions
$\square'$	Perturbation relative to time average
$\widetilde{\square}$	Mean-to-peak perturbation amplitude

References

[1] Dring, R., Blair, M., and Joslyn, H., 1980. "An Experimental Investigation of Film Cooling on a Turbine Rotor Blade". *J. Eng. Power,* ***102***(1), pp. 81–87.

[2] Takeishi, K., Aoki, S., Sato, T., and Tsukagoshi, K., 1992. "Film Cooling on a Gas Turbine Rotor Blade". *J. Turbomach.,* ***114***(4), pp. 828–834.

[3] Bunker, R., 2017. "Evolution of Turbine Cooling". IGTI Scholar Lecture*, ASME Paper No. GT2017-63205*.

[4] Mehendale, A. B., Han, J.-C., Ou, S., and Lee, C., 1994. "Unsteady Wake Over a Linear Turbine Blade Cascade With Air and CO_2 Film Injection: Part II—Effect on Film Effectiveness and Heat Transfer". *J. Turbomach.,* ***116***(4), pp. 730–737.

[5] Funazaki, K., Yokota, M., and Yamawaki, S., 1997. "Effect of Periodic Wake Passing on Film Effectiveness of Discrete Cooling Holes Around the Leading Edge of a Blunt Body". *J. Turbomach.,* ***119***(2), pp. 292–301.

[6] Saumweber, C., and Schulz, A., 2012. "Free-Stream Effects on the Cooling Performance of Cylindrical and Fan-Shaped Cooling Holes". *J. Turbomach.,* ***134***(6), p. 061007.

[7] Womack, K. M., Volino, R. J., and Schultz, M. P., 2008. "Measurements in Film Cooling Flows with Periodic Wakes". *J. Turbomach.,* ***130***(4), p. 041008.

[8] Heidmann, J. D., Lucci, B. L., and Reshotko, E., 2001. "An Experimental Study of the Effect of Wake Passing on Turbine Blade Film Cooling". *J. Turbomach.,* ***123***(2), pp. 214–221.

[9] Ligrani, P., Gong, R., Cuthrell, J., and Lee, J., 1996. "Bulk flow pulsations and film cooling—II. Flow structure and film effectiveness". *Int. J. Heat Mass Transfer,* ***39***(11), pp. 2283–2292.

[10] Seo, H. J., Lee, J. S., and Ligrani, P. M., 1999. "Effects of Bulk Flow Pulsations on Film Cooling From Different Length Injection Holes at Different Blowing Ratios". *J. Turbomach.,* ***121***(3), pp. 542–550.

[11] Abhari, R. S., and Epstein, A. H., 1994. "An Experimental Study of Film Cooling in a Rotating Transonic Turbine". *J. Turbomach.,* ***116***(1), pp. 63–70.

[12] Abhari, R. S., 1996. "Impact of Rotor-Stator Interaction on Turbine Blade Film Cooling". *J. Turbomach.,* ***118***(1), pp. 123–133.

[13] Bernsdorf, S., Rose, M. G., and Abhari, R. S., 2008. "Experimental Validation of Quasisteady Assumption in Modeling of Unsteady Film-Cooling". *J. Turbomach.,* ***130***(1), p. 011022.

[14] Ligrani, P., Gong, R., Cuthrell, J., and Lee, J., 1996. "Bulk flow pulsations and film cooling—I. Injectant behavior". *Int. J. Heat Mass Transfer,* ***39***(11), pp. 2271–2282.

[15] Brandvik, T., and Pullan, G., 2011. "An Accelerated 3D Navier–Stokes Solver for Flows in Turbomachines". *J. Turbomach.,* ***133***(2), p. 021025.

[16] Kim, S., Pullan, G., Hall, C., Grewe, R., Wilson, M., and Gunn, E., 2018. "Stall Inception in Low Pressure Ratio Fans". *ASME Paper No. GT-2018-75153*.

[17] Grimshaw, S., Pullan, G., and Hynes, T. P., 2016. "Modeling Nonuniform Bleed in Axial Compressors". *J. Turbomach.,* ***138***(9), p. 091010.

[18] Rowbury, D., Oldfield, M., and Lock, G., 2001. "A Method for Correlating the Influence of External Crossflow on the Discharge Coefficients of Film Cooling Holes". *J. Turbomach.,* ***123***(2), pp. 258–265.

[19] Day, C., Oldfield, M., and Lock, G., 2000. "Aerodynamic performance of an annular cascade of film cooled nozzle guide vanes under engine representative conditions". *Exp. Fluids,* ***29***(2), pp. 117–129.

[20] Johnson, R., Maikell, J., Bogard, D., Piggush, J., Kohli, A., and Blair, M., 2009. "Experimental Study of the Effects of an Oscillating Approach Flow on Overall Cooling Performance of a Simulated Turbine Blade Leading Edge". *ASME Paper No. 2009-GT-60290*.

[21] Meyer, R., 1958. "The Effect of Wakes on the Transient Pressure and Velocity Distributions in Turbomachines". *J. Basic Eng.,* ***80***(7), pp. 1544–1552.

[22] Kachel, C. E., and Denton, J. D., 2006. "Experimental and Numerical Investigation of the Unsteady Surface Pressure in a Three-Stage Model of an Axial High Pressure Turbine". *J. Turbomach.,* ***128***(2), pp. 261–272.

[23] Denton, J. D., 2002. "The Effects of Lean and Sweep on Transonic Fan Performance". *Task Quarterly,* ***6***(1), pp. 7–23.

[24] Oldfield, M., 2008. "Impulse Response Processing of Transient Heat Transfer Gauge Signals". *J. Turbomach.,* ***130***(2), p. 021023.

[25] O'Dowd, D., Zhang, Q., He, L., Ligrani, P., and Friedrichs, S., 2011. "Comparison of Heat Transfer Measurement Techniques on a Transonic Turbine Blade Tip". *J. Turbomach.,* ***133***(2), p. 021028.